Overcoming temperature polarization in membrane distillation by thermoplasmonic effects activated by Ag nanofillers in polymeric membranes

Antonio Politano[a], Gianluca Di Profio[b], Enrica Fontananova[b], Vanna Sanna[c], Anna Cupolillo[d], Efrem Curcio[b,e,*]

[a] Fondazione Istituto Italiano di Tecnologia, Graphene Labs, via Morego, 30, 16163 Genova, Italy
[b] Institute on Membrane Technology, National Research Council of Italy ITM-CNR, Italy - Via P. Bucci Cubo 17C, 87036 Rende, CS, Italy
[c] Nanomater S.r.l., Porto Conte Ricerche, Loc. Tramariglio, 07041 Alghero, SS, Italy
[d] Department of Physics, University of Calabria, Via P. Bucci Cubo 31C, 87036 Rende, CS, Italy
[e] Department of Environmental and Chemical Engineering DIATIC, University of Calabria, Via P. Bucci Cubo 45A, 87036 Rende, CS, Italy

A B S T R A C T

In recent years, Membrane Distillation (MD) has emerged either as a promising alternative or as a complement to Reverse Osmosis (RO) in seawater desalination. However, the performance of MD is significantly offset by temperature polarization, a phenomenon intrinsically related to water evaporation that causes the decrease of the solution temperature at the membrane surface and, ultimately, the loss of driving force. In this work, we show that temperature polarization can be withdrawn by exploiting thermal collective effects activated by the excitation of plasmonic modes in UV-irradiated Mixed Matrix Membranes composed of silver nanoparticles (Ag NPs) incorporated in polyvinylidene fluoride (PVDF) microporous films. For experimental tests carried out under vacuum (VMD) and with an absorbed radiant heating power of $2.3 \cdot 10^4$ W/m^2, best results were obtained using PVDF membranes loaded with 25%Ag NPs. In this case, measured transmembrane fluxes to pure water and 0.5 M NaCl solution were 32.2 and 25.7 L/m^2 h, respectively, i.e. about 11- and 9- fold higher than the corresponding values for unloaded membranes. Remarkably, energy analysis revealed that the heat generation of Ag NPs under plasmonic resonance was able to withdrawn temperature polarization, resulting in estimated temperature polarization factor (TPF) values of 106.5% for 0.5 M NaCl solution.

1. Introduction

In recent years, Membrane Distillation (MD) has emerged as a promising alternative or as a complementary unit to Seawater Reverse Osmosis (SWRO). MD is a thermally-driven membrane operation based on the use of microporous hydrophobic membranes [1]. The hydro-repellent nature of the membrane prevents the permeation of liquids, while sustaining a vapor-liquid interface at the entrance of each pore, where water evaporation takes place. Under a temperature gradient, a net diffusive flux of vapor is observed from the hot feed compartment to the opposite side of the membrane (distillate compartment) [2–4].

In desalination applications, MD is able to produce desalted water at high purity since, theoretically, non-volatile compounds (ions, colloids, and macromolecules) are completely retained by the membrane. In addition, MD is unlimited by polarization phenomena and, therefore, recovery factors > 85% can be achieved [5].

Low temperature gradients are usually adequate to obtain a trans-membrane flux of 1–10 L/m^2 h with feed temperatures spanning between 50 and 70 °C, thus permitting the effective recovery of low-grade or waste heat streams, along with the exploitation of alternative energy sources (solar, wind or geothermal) [6].

Presently, the main drawback of MD is represented by "temperature polarization", a phenomenon inherently related to the removal of the latent heat associated to water evaporation, which causes the progressive decline of the feed temperature profile in proximity to the membrane surface. As a result, the temperature at the membrane interface is lower than the bulk temperature and, consequently, the net driving force to the mass transport falls down.

Some technological solutions have been proposed so far in order to alleviate the negative impact of temperature polarization. Since polarization phenomena are localized within the micrometric boundary layer adjacent to the membrane, improved hydrodynamic conditions

(increase of Reynolds number, applying turbulence promoters like spacers) are somehow beneficial for the simultaneous mass and heat transfer in MD [7,8]. Hengl et al. [9] have manufactured and tested flat hydrophobic metallic membranes for water evaporation in an operational configuration approaching sweep gas MD; here, the membrane acts as an electric resistance that brings energy directly to pores by Joule effect [9].

However, due to the negative impact represented by temperature polarization on the overall thermal efficiency, the effective technological implementation of MD on large industrial scale is missing yet.

As a result of a multidisciplinary cooperation with solid-state physicists active in the field of plasmonics, here we propose an innovative technological approach to reduce or withdraw temperature polarization. In thermoplasmonics [10–14], the photoexcitation of plasmons in metal nanoparticles (NPs) [15–17] is exploited to obtain a local increase of the temperature [18]. The presence of nanoscale thermal hotspots has been demonstrated to be beneficial for different applications in membrane technology [19], including MD [20]. However, the physical mechanism ruling thermoplasmonic MD have not been clarified yet. As a matter of fact, different experimentalists [21,22] have shown that, upon illuminating an extensive quantity of Au NPs dispersed in solution, the temperature profile is not localized around each NP, as a consequence of the occurrence of thermal collective effects [23]. The distribution of the temperature becomes nearly constant throughout the NP assembly, regardless the nanoscopic size of heat sources [23]. While applications in nanotechnology could be inhibited by such collective thermal effects, actually they are even advantageous in membrane technology, where nano-heaters have the potential to provide a temperature increase in a large area, leading to a significant enhancement of the mass transfer.

In this work, a quantitative evaluation of temperature polarization and energy efficiency is provided for a vacuum MD (VMD) system operated with microporous Mixed Matrix Membranes (MMM) made in PVDF and incorporating Ag NPs. UV-irradiation of MMMs allowed exploiting thermal collective effects activated by the excitation of plasmons. Process performance in terms of transmembrane flux and permeate quality is also investigated.

2. Theoretical background

VMD configuration implies a suppression of the heat flux at the vacuum/permeate interface [4]. Consistently, temperature gradient is negligible along the membrane thickness. Therefore, the heat required for the evaporation of water molecules at the feed interface is supplied by the heat flux through the liquid film adjacent to the membrane at the feed side [18]. However, in our innovative system, the presence of Ag nanofillers in the polymeric membrane leads to an additional term associated to the thermoplasmonic heat flux (q_{plasm}), which considers the increase of membrane temperature at the feed interface under UV irradiation:

$$h_f(\overline{T}_f^b - \overline{T}_f^m) + q_{plasm} = J_w \lambda \tag{1}$$

where superscript m refers to membrane interface, $\overline{T}_f$ is the average feed temperature (arithmetic average between inlet and outlet temperature), h_f is the heat transfer coefficient at the feed side, J_w is the transmembrane flux of vapor and λ is the latent heat of vaporization. From Eq. (1), the average value of temperature at the membrane interface $\overline{T}_f^m$ is evaluated to be:

$$\overline{T}_f^m = \overline{T}_f^b + \frac{q_{plasm} - J_w \lambda}{h_f} \tag{2}$$

The heat transfer coefficient at the feed side can be estimated by the Hausen empirical correlation valid for Re < 2300 and Pr ≥ 5:

$$Nu = 3.66 + \frac{0.688 RePr(d/L)}{1 + 0.44[RePr(d/L)]^{2/3}} \tag{3}$$

where Nu, Re and Pr are the Nusselt, Reynolds and Prandtl dimensionless numbers, respectively, and (d/L) is the tube diameter-to-length ratio.

The thermoplasmonic heat flux is experimentally determined by a macroscopic energy balance over the whole system, considering that the sum of q_{plasm} and of the heat flux associated to the radiation of the UV lamp q_{rad} (the latter is measured in a VMD cell equipped with virgin PVDF membrane, i.e. $q_{plasm} = 0$) balances the sum of the heat flux associated to water evaporation (obtained by multiplying the measured transmembrane flux J_w and the latent heat of water λ) and of the heat flux through the liquid feed stream (obtained by multiplying the feed flowrate $\dot{m}_f$, the specific heat coefficient c_p and the measured temperature increase from inlet to outlet $T_{f,\,out}^b - T_{f,\,in}^b$). Hence:

$$q_{plasm} = J_w \cdot \lambda + \dot{m}c_p(T_{f,out}^b - T_{f,in}^b) - q_{rad} \tag{4}$$

3. Materials and methods

3.1. Membrane preparation and characterization

Ag NPs were synthesized by the chemical reduction method using sodium citrate as metal precursor [24]. In a usual batch, AgNO$_3$ salt (Sigma-Aldrich, US) was first dissolved into water (100 mL of aqueous solution at concentration of 1 mM) and successively heated up. Once reached the boiling point, an aqueous solution of trisodium citrate (10 mL, 1 wt%) was added, in order to reduce Ag$^+$ ions to produce Ag NPs. Consistently, the colloidal solution assumed a light yellow tint. The obtained NPs were instantly lyophilized and stored at room temperature. Size and shape of Ag NPs were characterized by transmission electron microscopy (TEM, FEI Tecnai G12, US). Spherical NPs with average diameter of 31 ± 4 nm with rather uniform size distribution are shown in Fig. 1. Ag NPs were dispersed in Dimethylformamide (DMF) bought from Sigma-Aldrich (US) at 30% w/w. UV-VIS analysis performed on a solution sample diluted 200 times evidenced a maximum absorbance intensity at ~420 nm, corresponding to the wavelength of the plasmonic resonance in Ag NPs [25].

Flat microporous membranes with Ag nanofillers were prepared by nonsolvent-induced phase inversion process. The mix of Ag NPs in DMF was firstly sonicated for 15 min (M 428-BD, MPM Instruments Srl) at room temperature, and successively mixed with PVDF homopolymer powder Solef®6010 (Solvay, Italy). Proper amount of pure DMF was added in order to modulate the final concentration of Ag NPs in the range of 15–25% w/w. After 24 h of magnetic stirring at 30 °C, the polymeric solution was cast on a glass plate by automated machine (Elcometer, UK) using a knife with gap of 150 μm, and then immersed for 2 h at room temperature in a coagulation bath of distilled water to activate demixing. Residual traces of solvents were removed by another immersion in distilled water (for one day), followed by a washing with ethanol. Membranes were dehydrated in oven at 60 °C under vacuum for one day. The morphology of membranes was studied by a Quanta 200 FEI (Philips, Netherlands) scanning electron microscope. Experiments for evaluating the contact angle were performed by CAM 200 contact angle meter (KSV Instruments LTD, Finland). Pore size distribution was determined by Capillary Flow Porometer (CFP 1500 AEXL, PMI Inc., US).

3.2. VMD setup and testing

The VMD setup schematized in Fig. 2 consists of a dead-end cell with an active membrane area of 21.2 cm^2. A quartz window was fixed and taped up at the middle of the upper cap. Above the quartz window, in order to irradiate the surface of the membrane, we put a high-pressure UV mercury lamp (Helios Ital Quarz srl, Italy) with a wavelength
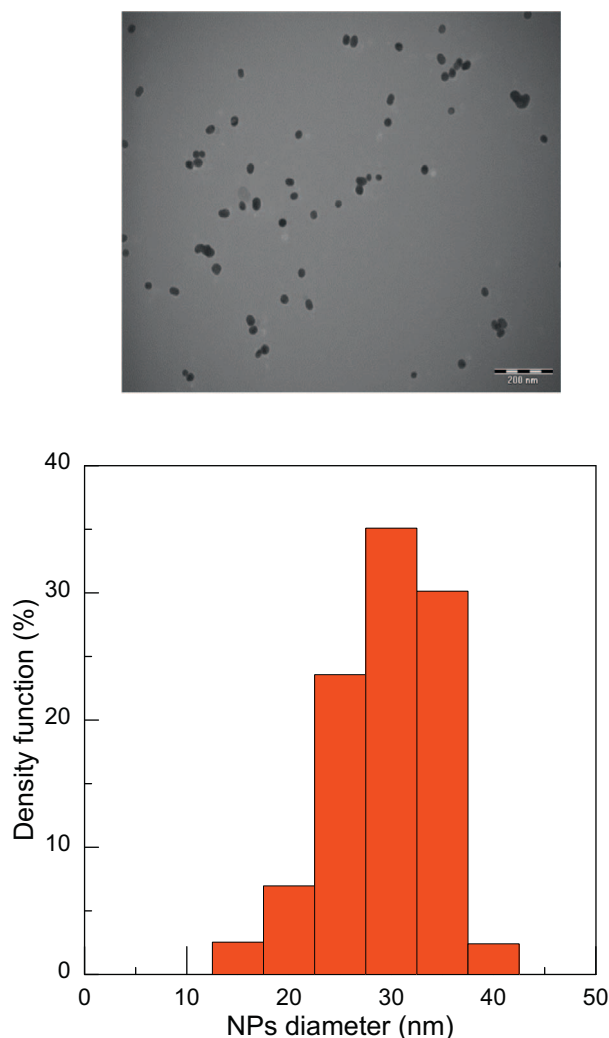
Fig. 1. (top panel) TEM image and (bottom panel) distribution function of the particle size of synthesized Ag NPs.

$$J_w = \frac{\Delta W}{A \cdot \Delta t} \qquad (5)$$

Permeate conductivity was evaluated by conductivity meter at 20 °C (YSI Model 3200). Dynamic Light Scattering/DLS (90Plus Particle Size Analyzer, Brookhaven Instruments Corporation, US) and High-Resolution Continuum Source Atomic Absorption Spectrometer/HR-CS AAS (ContrAA 700, Analytik Jena AG, Germany) were used to demonstrate the absence in the permeate of solid and dissolved (in the form of Ag^+ ions) NPs, respectively.

In addition to pure water and 0.5 M NaCl solution artificially mimicking seawater, VMD tests were also carried out on real seawater. Raw samples from Tyrrenian sea (Amantea, Italy) were collected and stored at 4 °C before use. Ion Chromatography (Metrohm 861 Advanced Compact Ion Chromatograph) was employed to quantify the concentration of ions in both feed and distillate streams; 3.2 mM Na_2CO_3 + 1 mM $NaHCO_3$ was used as eluent for anion column Metrosep A Supp 5–250/4.0, and 2 mM nitric acid + 0.25 mM oxalic acid was used as eluent for cation column Metrosep C4–250/4.0. The organic content in real seawater and permeate solutions of CO_2-free solutions by a Total Organic Carbon (TOC) analyzer (Shimadzu VCSN). Conductivity of solutions was measured by YSI model 3200 Conductivity Instrument (US). We measured pH by HI 223 Calibration-Check Microprocessor pH Meter (HANNA Instruments, US).

4. Results and discussion

4.1. Performance of membranes

Table 1 summarizes the morphological and physicochemical properties of NP-loaded PVDF membranes. SEM micrographs proved that Ag NPs, entrapped in the lab-made membranes during the non-solvent phase inversion process, were well dispersed throughout the PVDF microporous matrix. Specifically, the cross-section morphology appeared asymmetric, with a outermost layer displaying macrovoids generally protracted over 40% c.a. of the membrane thickness, and with a steady microporous structure at the bottom layer. While thickness was almost uniform (spanning from 60 to 72 μm), the porosity of unloaded PVDF membranes progressively increased with the amount of incorporated NPs (up to 20%w/w), as a result of their hetero-nucleant effect, which accelerates the kinetics of solid phase formation. However, for PVDF-25% Ag NPs, the porosity reached the lowest value (22%), probably due to a partial collapse of the membrane structure. As evaporation tests were carried out under vacuum and with non-pressurized feed stream, no significant variations of the pore size were detected after 6 months of experimental activities.

With the aim to validate the stability of membranes against NPs dissolution with subsequent Ag^+ release, samples of PVDF-Ag NPs polymeric films (surface area of 2 cm^2) were immersed (i) in pure water and (ii) in 0.5 M NaCl for one week at 20 °C. Ion concentration was checked by HR-CS AAS.

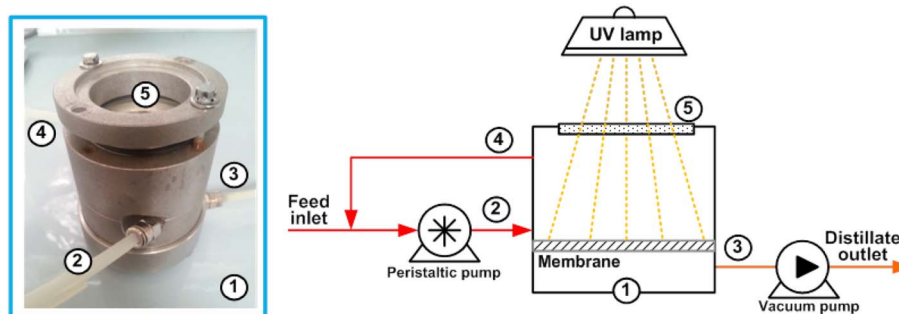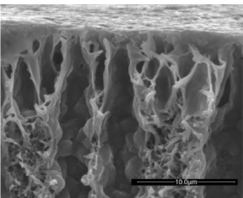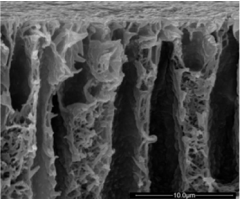According to dissolution data reported in Table 2, the highest Ag^+

of 366 nm, a watching angle of 90° and with a GR.E. 500 W portable power generator. The recirculation of the feed solution (0.5 M NaCl) was carried out at 20 L/h by digital peristaltic pump Masterflex L/S (Cole Parmer, US). Temperature monitoring at inlet and outlet of the module was performed by means of K-type thermocouples, characterized by a response time of 15 s and a resolution of ± 0.1 °C. The operative pressure of the distillate side was 20 mbar; the initial feed temperature was set to 30 °C.

The transmembrane flux of water vapor J_w was evaluated by computing the weight decrease (ΔW) of the feed solution in a fixed interval of time (Δt) and normalizing it over the membrane area A:
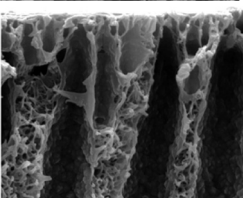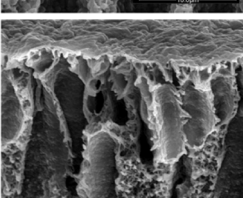

Fig. 2. Lab-scale experimental setup. (1) VMD unit; (2) feed inlet stream; (3) feed outlet stream; (4) distillate outlet stream; (5) glass window for UV irradiation.

Table 1
Morphological and physicochemical properties of investigated PVDF membranes. The scale bar in SEM images represents 10 μm.

Membrane	Morphology (SEM micrographs)	Thickness (μm)	Porosity (%)	Pore size (μm)	Contact angle (°)
Virgin PVDF		64 ± 11	27	0.45 ± 0.05[†] 0.45 ± 0.06[‡]	86.3 ± 2.5[†] 86.5 ± 3.4[‡]
PVDF-15%Ag NPs		72 ± 14	32	0.22 ± 0.03[†] 0.21 ± 0.05[‡]	83.6 ± 3.9[†] 84.1 ± 2.8[‡]
PVDF-20%Ag NPs		65 ± 12	36	0.38 ± 0.04[†] 0.37 ± 0.02[‡]	81.4 ± 0.7[†] 82.0 ± 2.5[‡]
PVDF-25%Ag NPs		60 ± 15	22	0.40 ± 0.05[†] 0.38 ± 0.04[‡]	80.3 ± 3.6[†] 80.6 ± 3.1[‡]

[†] Before VMD tests.
[‡] After 6 months.

Table 2
Dissolution tests of Ag NPs in MMM.

Membrane	Pure water	0.5 M NaCl
	Dissolved Ag$^+$ (ppb)[†]	Dissolved Ag$^+$ (ppb)[†]
PVDF-15%Ag NPs	3.4 ± 0.08	69.8 ± 2.41
PVDF-20% Ag NPs	9.9 ± 0.27	126.0 ± 5.95
PVDF-25% Ag NPs	14.0 ± 0.68	138.0 ± 6.50

[†] After 7-days immersion at 20 °C. Average values on 3 samples, standard deviation < 5%.

concentration in water - detected for PVDF-25% Ag NPs membrane - is about three orders of magnitude lower than AgOH solubility. In general, these values are lower than those reported in literature and related to the solubilization of Ag NPs dispersed in water, as a result of the shielding effect of the hydrophobic polymeric matrix [26]. The increment of dissolution rate of Ag NPs in 0.5 M NaCl solution is in agreement with previous studies [26,27].

Incorporation of citrate-capped Ag NPs into PVDF matrix reduced the contact angle to water: as the percentage of Ag NPs increased from 0 to 25%, an overall reduction of the contact angle by ~7% (down to 80.3 ± 3.6°) was observed. Remarkably, only a very small increase of contact angle was noticed after 6 months, presumably due to the aforementioned slight dissolution of Ag NPs.

The heat power Q_i carried by the single i-th NP is directly related to its absorption cross section σ_{abs} by the following relation [14]:

$$Q_i = \sigma_{abs} n_s \varepsilon_0 c \ |E^{ext}|^2/2 \tag{6}$$

where n_s is the refraction index of the neighbouring medium, c is the speed of light, and E^{ext} is the electric field of the external electromagnetic radiation. Thus, the choice of the material for plasmonic nanofillers is orientated toward systems that exhibit high values of the absorption cross section σ_{abs} under resonance conditions for plasmonic excitations. Based on the state of the art, the materials showing the best performances concerning photothermal effects are Ag and Au [14,28]. However, shape-controlled Ag NPs [29], under plasmon resonance conditions, can generate a heat flux about ten times more than Au NPs [28]. In addition, by appropriately selecting the synthesis procedure [29], it is possible to control the size and the shape of Ag NPs. Accordingly, our synthesis method allowed us (see Section 3.1) to obtain NPs with diameter of ~30 nm (Fig. 1) in order to maximize photothermal effects.

Ultraviolet-visible (UV–Vis) spectra of manufactured membranes (Fig. 3) demonstrated that the maximum absorbance intensity is slightly affected by the polymeric matrix, ranging between 420 and 440 nm, coherently with the wavelength of the plasmonic resonance of Ag NPs [30].

Fig. 4 illustrates the difference between outlet and inlet feed temperature for 0.5 M NaCl solution, as resulting from the heat flux associated to the radiation of the UV lamp and the thermoplasmonic effects of irradiated Ag NPs. The temperature difference gradually increased with time, getting a stationary behavior in about 30 min for the VMD setup used. When the cell was operated with unloaded PVDF membranes ($q_{plasm} = 0$), the energy associated to the UV radiation
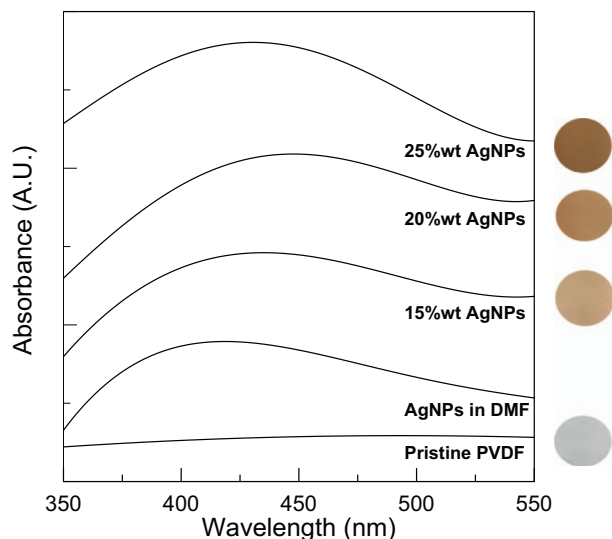
Fig. 3. UV–Vis characterization of mixed matrix PVDF membranes incorporating different amounts of Ag NPs. The color gradation of membrane surface, from white to brown, as a function of NP content is shown on the left side. (For interpretation of the references to color in this figure legend, the reader is referred to the web version of this article.)
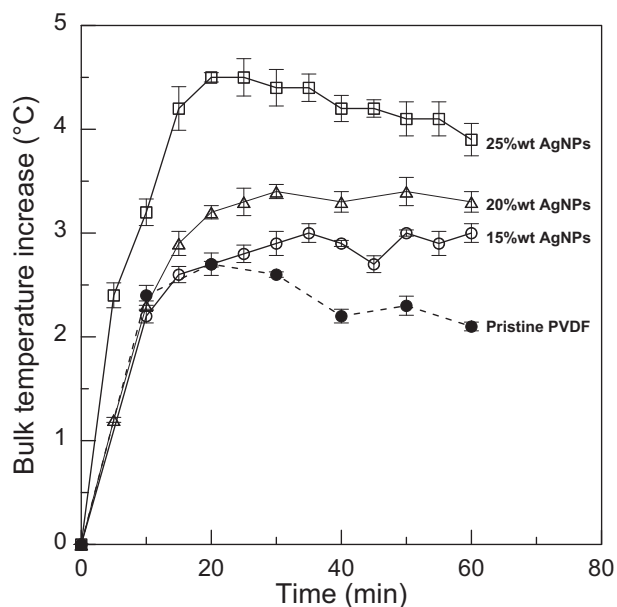

Fig. 4. Time-dependent difference between outlet and inlet feed temperature (30 °C) for 0.5 M NaCl solution.

determined a temperature difference by ~2.5 °C. For PVDF membranes loaded with Ag NPs, the illumination of metal NPs with wavelength close to their plasmonic resonance turned them into local nano-heaters, thus determining an enhancement of the outlet feed temperature. This thermoplasmonic effect increased with Ag content: the highest temperature increase, i.e. ~4 °C, was detected for PVDF-25% Ag NPs membrane.

Transient transmembrane flux profiles measured over an operation time of 1 h are illustrated in Fig. 5 for both pure water (panel a) and 0.5 M NaCl solution (panel b). Vapor fluxes through unloaded PVDF are noticeably lesser than through MMM embedding NP fillers. Specifically, fluxes through PVDF-25% Ag NPs, evaluated at one hour, are about nine-fold (feed: 0.5 M NaCl solution) and eleven-fold (feed: H$_2$O) greater with respect to the corresponding values for virgin PVDF membranes.

The analysis of structural characteristics shown in Table 1 clearly indicates that the extent of morphological variations associated to the addition of nanofillers in the membranes (primarily in terms of porosity and pore size) is not enough to explain the noteworthy improvement of the transmembrane flux, which conversely is determined by thermo-plasmonic effects.

4.2. Energy analysis

The study of temperature changes at the membrane interface, due to polarization phenomenon, as a function of the NP content can shed light on the influence of photothermal plasmonic excitation on the overall MD performance. A temperature polarization factor (*TPF*) is defined as:

$$TPF = \frac{\overline{T}_f^m}{\overline{T}_f^b} \times 100 \tag{7}$$

with *TPF* < 100 in conventional VMD.

While bulk temperature was experimentally measured, interfacial temperature was estimated by Eq. (2). The *TPF*, predicted for unloaded PVDF membrane ($q_p = 0$) under the operating conditions adopted in this study, was 99.35% for pure water and 98.25% for 0.5 M NaCl solution. For salt solution, the lower TPF reflects the lower heat transfer coefficient (660 W/m^2 h) with respect to pure water (1010 W/m^2 h). The thermal energy produced by plasmonic nanofillers reversed the polarization effect, leading (i) to an interface feed temperature higher that in the bulk and (ii) to a *TPF* > 100%. Fig. 6 displays the behavior of the *TPF* (squares) as a function of the content of Ag NPs for VMD tests on 0.5 M NaCl solution. It is evident that, by increasing the amount of Ag NPs, the *TPF* increases up to values higher than 106; likewise, the interfacial temperature (circles) increases with the amount of Ag NPs.

To understand experimental results shown in Figs. 4–6, one has to consider that - when illuminating a large amount of metal NPs dispersed in a medium - the temperature profile throughout the system may no longer be localized around each NP as nanometric source of heat, due to thermal collective effects [21,22]. Baffou et al. [23] built a theoretical model for reproducing the temperature distribution throughout large assemblies of metal NPs. In details, they considered two well-distinct regimes: (i) the "temperature confinement regime" with a temperature distribution essentially confined at the vicinity of each NP and (ii) a "delocalization regime" characterized by a smooth temperature profile throughout the surrounding medium [23]. Therefore, the total temperature increase ΔT experienced by the system is given by the sum of a term ΔT^s associated to the self-contribution of a single nano-heater, and of a term ΔT^{ext} due to the heat delivered by the other NPs located in proximity of the NP. Specifically:

$$\Delta T_0^s = \frac{2 \cdot \sigma_{abs} \cdot I}{4\pi \overline{k} d} \tag{8}$$

and, for uniform and circular illumination of an infinite array:

$$\Delta T_0^{ext} \approx \frac{\sigma_{abs} \cdot I}{\overline{k}} \frac{1}{4} \frac{D}{A} \left(1 - \frac{2\sqrt{A}}{\sqrt{\pi} D} \right) \tag{9}$$

where subscript "0" identifies the center of an ensemble of plasmonic NPs.

By considering a NP diameter d of 30 nm, an approximate inter-particle distance p of $2 \cdot 10^{-7}$ m for PVDF-25% Ag NPs, a unit cell area A for a NP square lattice of $p^2 = 4 \cdot 10^{-14}$ m^2, an irradiance I of $2.3 \cdot 10^4$ W/m^2, a diameter of the irradiated area D of $5.2 \cdot 10^{-2}$ m, an average thermal conductivity $\overline{k}$ of 0.37 W/mK (estimated by the arithmetic average between the thermal conductivity of PVDF membrane with porosity of 0.22 [3] and water), and a NP absorption cross section σ_{abs} of $2 \cdot 10^{-15}$ m^2 [31], the total ΔT is estimated to be ~42 K. Under these assumptions, the self-contribution term ΔT_0^s is largely negligible with respect to collective effects produced by the lattice of NPs. Since
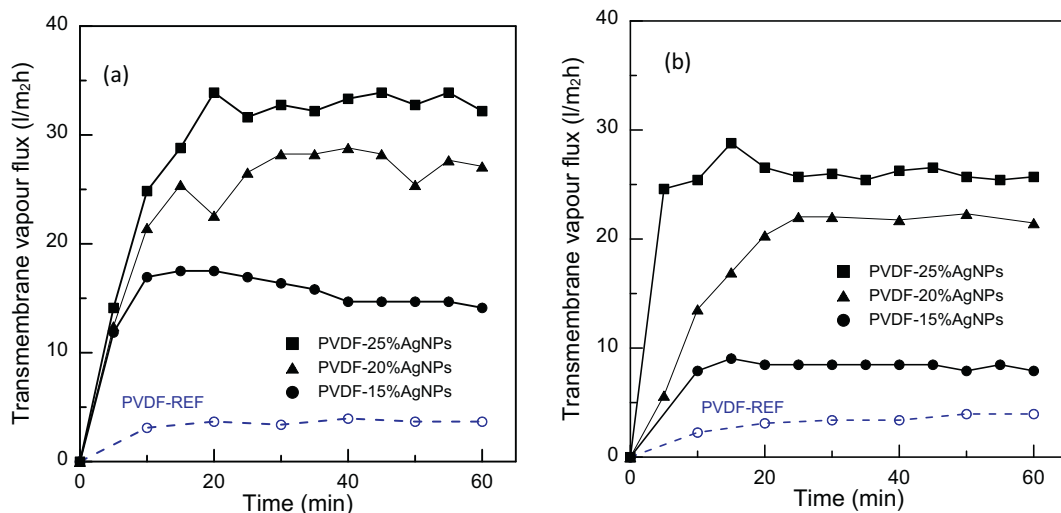
Fig. 5. Time-dependent profile of the transmembrane flux through PVDF membranes loaded with different amounts of Ag nanofillers. PVDF-REF denotes the unloaded PVDF membrane assumed as a reference. The feed is: (a) pure H_2O; (b) 0.5 M NaCl.
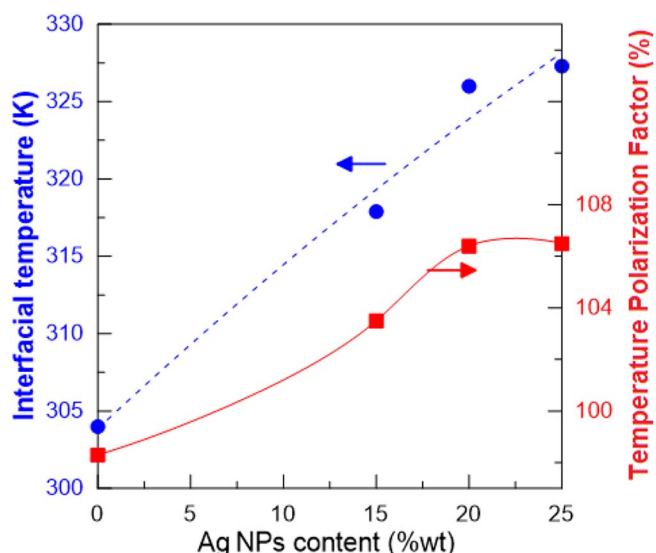

Fig. 6. Steady-state behavior of the interfacial temperature (circles) and *TPF* (squares) as a function of the content of Ag NPs entrapped in PVDF membranes. Feed: 0.5 M NaCl solution.

Eqs. (8) and (9) do not take into account the cooling effect associated to water evaporation at the membrane interface, the predicted value of ΔT is obviously higher than the increase of bulk temperature estimated by energy balance in the VMD unit as per Eq. (2), i.e. 23.3 K for PVDF-25% Ag NPs operated on 0.5 M NaCl solution (see Fig. 6). However, this theoretical approach provides a useful tool for outlining the potentialities of plasmonics in thermal processes occurring at solid-liquid interfaces.

Fig. 7 quantitatively illustrates the different terms of the energy balance expressed by Eq. (4). Interestingly, for tests with pure water, data show that the plasmonic heat flux overcomes by about 1.7-fold the heat flux associated to the evaporation through MMM, doubling for 0.5 M NaCl solution.

Energy efficiency (*EE*) provides a quantitative estimation of the percentage of the heat stream (absorbed UV radiant flux and plasmonic heat flux) that is effectively used to promote water evaporation through the membrane. *EE* is thus defined as:

$$EE = \frac{\text{Evaporation Heat Flux}}{\text{Total Heat Flux}} = \frac{J_w \lambda A}{\dot{m} c_p (T_{f,out}^b - T_{f,in}^b) + J_w \lambda A} \quad (10)$$
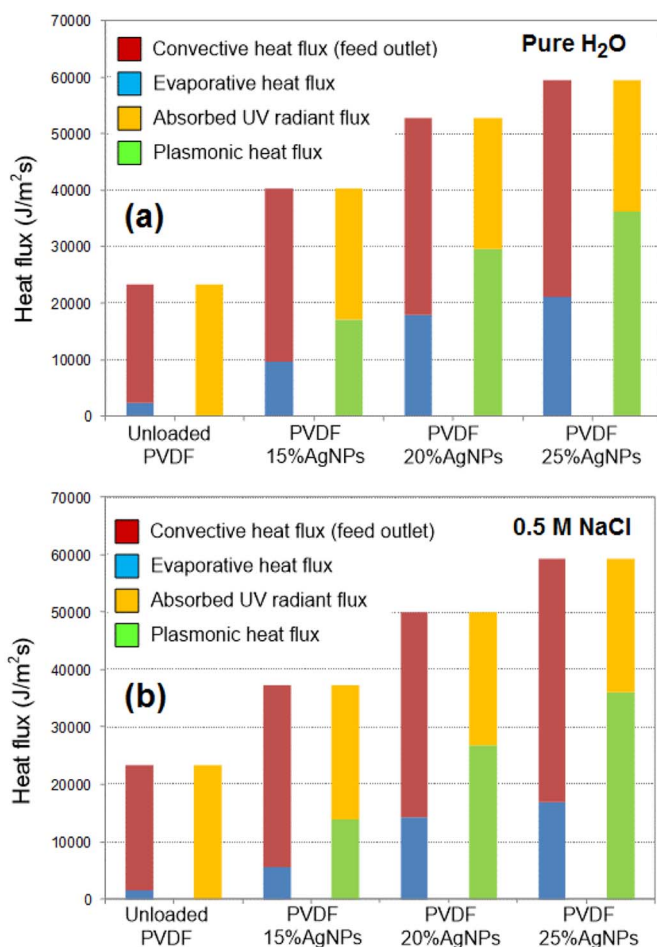

Fig. 7. Heat fluxes in thermoplasmonic VMD. Feed: (a) pure H_2O; (b) 0.5 M NaCl solution.

where A is the membrane area. *EE* is enhanced at increasing concentration of NPs within the membrane matrix, reaching a maximum of 32.1% and 28.1% when using pure water and 0.5 M NaCl as feed stream, respectively (Table 3). The exceeding energy merely increases the temperature of the feed outlet stream and might be recovered by conventional heat exchanger systems or innovative salinity gradient power technologies [32].

Table 3
Energy analysis for thermoplasmonic VMD.

Feed	Membrane	*EE* (%)
Pure water	PVDF-REF	8.10
	PVDF-15% Ag NPs	20.6
	PVDF-20% Ag NPs	30.0
	PVDF-25% Ag NPs	32.1
0.5 M NaCl	PVDF-REF	6.06
	PVDF-15% Ag NPs	14.9
	PVDF-20% Ag NPs	28.1
	PVDF-25% Ag NPs	28.4

Table 4
Chemical composition of feed seawater (Tyrrenian sea, location: Amantea, Italy).

pH	8.0
Temperature (°C)	25
Density (kg/l)	1.02
Ca^{2+} (ppm)	492.5
Mg^{2+} (ppm)	2120.7
Na^+ (ppm)	11,941
K^+ (ppm)	348
Cl^- (ppm)	20,975
Br^- (ppm)	116.5
HCO_3^- (ppm)	140
SO_4^{2-} (ppm)	2192
Conductivity (µS/cm)	68,000
TOC (mg/l)	4.1
Silt density index (SDI$_{15}$)[†]	2.4
Water activity	0.97

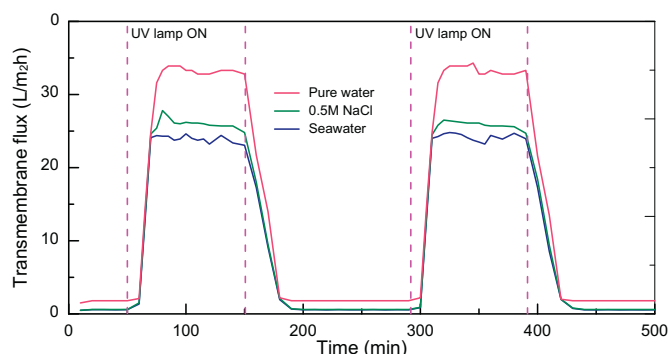[†] SDI$_{15}$ measurement procedure from ASTM standard test method D 4189-82.

Fig. 8. Transmembrane flux of vapor through a 25% w/w Ag-NPs loaded PVDF membrane. Feed typology: pure water, 0.5 M NaCl and real seawater.

4.3. Permeate quality

Analytical tests were carried out on distillate samples in order to check the quality of desalted water. Incorporation of citrate-capped Ag NPs into PVDF matrix, although decreasing moderately the value of water contact angle (Table 1), did not cause pore wetting: in experimental tests carried out on both pure water and 0.5 M NaCl solution, protracted over 7 days/10 h of operation per day, the permeate conductivity ranged within 0.9–2.1 µS/cm, thus providing evidence of the negligibility of salt leakage. Additionally, concentration of Ag NPs and Ag^+ ions were below the detectability threshold of DLS and HR-CS AAS instruments, as a result of both the specific evaporative transport mechanism in MD (non-volatile Ag^+ ions dissolved in the feed stream are retained), and the peculiar VMD configuration, where condensed distillate is not directly in contact with the membrane.

No significant changes (< 5%) in terms of transmembrane flux were observed during 10-h experiments repeated over 6 months.

4.4. Tests on real seawater

The chemical composition of real seawater samples collected from Tyrrenian sea is reported in Table 4. VMD tests were carried out using PVDF-25% Ag NPs membrane, i.e. the one exhibiting the highest performance.

With respect to 0.5 M NaCl solution, the average vapor flux in a VMD experimental test cycled twice was 6% lower (Fig. 8). The slightly reduced water activity coefficient of real seawater (0.97), estimated by using PHREEQC speciation software [33], gives a partial explanation this result.

Analysis of the distillate revealed only traces of Na^+ (1.0 ppm), Mg^{2+} (0.12 ppm), Cl^- (1.8 ppm) and SO_4^{2-} (0.11 ppm). The low electrical conductivity (5.9 µS/cm), the negligible organic content (TOC = 0.013 mg/l) and the absence of dispersed colloidal NPs in the condensed permeate confirmed the good stability of the membrane against wetting.

5. Conclusions

In this work, we have applied the innovative concept of thermoplasmonics in order to prove that temperature polarization phenomenon in MD can be withdrawn by using UV-irradiated Ag NPs, acting as nano-heaters resonating at the Ag plasma frequency, so as to produce collective thermal effects. In principle, this preliminary application to seawater desalination opens the way to the exciting perspective of an eco-friendly and economically feasible membrane technology for solar steam generation.

By exploiting the inherent dependence of mass transfer on temperature gradient, we made a remarkable step-change in the fields of thermoplasmonics and MD, showing that membranes manufactured with hydrophobic polymers and filled with size-selected plasmonic NPs can provide remarkable improvement in the system performance, both in terms of transmembrane flux and thermal efficiency.

The stability of NPs-charged membranes is a crucial issue in water treatment operations. In our innovative system, the release of silver ions and NPs in the permeate was prevented by the shielding effect of the hydrophobic polymeric matrix and the peculiar VMD configuration, in which there is not a liquid distillate contacting the membrane. Note that the use of thermoplasmonic membranes could be also extended to a wide spectrum of applications where diffusion-driven separation mechanisms depends on temperature, beyond seawater desalination (see as an example, the reviews in Ref. [14,19]).

References

[1] E. Drioli, A. Ali, F. Macedonio, Membrane distillation: recent developments and perspectives, Desalination 356 (2015) 56.

[2] E. Drioli, A. Criscuoli, E. Curcio, Membrane contactors and catalytic membrane reactors in process intensification, Chem. Eng. Technol. 26 (2003) 975.

[3] E. Curcio, E. Drioli, Membrane distillation and related operations — a review, Sep. Purif. Rev. 34 (2005) 35.

[4] M.A.E.-R. Abu-Zeid, Y. Zhang, H. Dong, L. Zhang, H.-L. Chen, L. Hou, A comprehensive review of vacuum membrane distillation technique, Desalination 356 (2015) 1.

[5] P. Wang, T.-S. Chung, Recent advances in membrane distillation processes: membrane development, configuration design and application exploring, J. Membr. Sci. 474 (2015) 39.

[6] S. Al-Obaidani, E. Curcio, F. Macedonio, G. Di Profio, H. Al-Hinai, E. Drioli, Potential of membrane distillation in seawater desalination: thermal efficiency, sensitivity study and cost estimation, J. Membr. Sci. 323 (2008) 85.

[7] L. Martínez-Díez, M.I. Vazquez-Gonzalez, Temperature and concentration polarization in membrane distillation of aqueous salt solutions, J. Membr. Sci. 156 (1999) 265.

[8] A. Ali, F. Macedonio, E. Drioli, S. Aljlil, O. Alharbi, Experimental and theoretical evaluation of temperature polarization phenomenon in direct contact membrane

distillation, Chem. Eng. Res. Des. 91 (2013) 1966.

[9] N. Hengl, A. Mourgues, M. Belleville, D. Paolucci-Jeanjean, J. Sanchez, Membrane contactor with hydrophobic metallic membranes: 2. Study of operating parameters in membrane evaporation, J. Membr. Sci. 355 (2010) 126.

[10] J.B. Herzog, M.W. Knight, D. Natelson, Thermoplasmonics: quantifying plasmonic heating in single nanowires, Nano Lett. 14 (2014) 499.

[11] M. Essone Mezeme, C. Brosseau, Engineering nanostructures with enhanced thermoplasmonic properties for biosensing and selective targeting applications, Phys. Rev. E 87 (2013) 012722.

[12] R. Rodríguez-Oliveros, J.A. Sánchez-Gil, Gold nanostars as thermoplasmonic nanoparticles for optical heating, Opt. Express 20 (2012) 621.

[13] M. Zhu, G. Baffou, N. Meyerbröker, J. Polleux, Micropatterning thermoplasmonic gold nanoarrays to manipulate cell adhesion, ACS Nano 6 (2012) 7227.

[14] G. Baffou, R. Quidant, Thermo-plasmonics: using metallic nanostructures as nanosources of heat, Laser Photonics Rev. 7 (2013) 171.

[15] Z. Liu, X. Liu, S. Huang, P. Pan, J. Chen, G. Liu, G. Gu, Automatically acquired broadband plasmonic-metamaterial black absorber during the metallic film-formation, ACS Appl. Mater. Interfaces 7 (2015) 4962.

[16] Z. Liu, P. Zhan, J. Chen, C. Tang, Z. Yan, Z. Chen, Z. Wang, Dual broadband near-infrared perfect absorber based on a hybrid plasmonic-photonic microstructure, Opt. Express 21 (2013) 3021.

[17] X. Chen, Y. Chen, M. Yan, M. Qiu, Nanosecond photothermal effects in plasmonic nanostructures, ACS Nano 6 (2012) 2550.

[18] Z.J. Coppens, W. Li, D.G. Walker, J.G. Valentine, Probing and controlling photothermal heat generation in plasmonic nanostructures, Nano Lett. 13 (2013) 1023.

[19] A. Politano, A. Cupolillo, G. Di Profio, H. Arafat, G. Chiarello, E. Curcio, When plasmonics meets membrane technology, J. Phys. Condens. Matter 28 (2016) 363003.

[20] A. Politano, P. Argurio, G. Di Profio, V. Sanna, A. Cupolillo, S. Chakaraborthy, H.A. Arafat, E. Curcio, Photothermal membrane distillation for seawater desalination, Adv. Mater. 29 (2017) 1603504.

[21] A.O. Govorov, W. Zhang, T. Skeini, H. Richardson, J. Lee, N.A. Kotov, Gold nanoparticle ensembles as heaters and actuators: melting and collective plasmon resonances, Nanoscale Res. Lett. 1 (2006) 84.

[22] H.H. Richardson, M.T. Carlson, P.J. Tandler, P. Hernandez, A.O. Govorov, Experimental and theoretical studies of light-to-heat conversion and collective heating effects in metal nanoparticle solutions, Nano Lett. 9 (2009) 1139.

[23] G. Baffou, P. Berto, E. Bermúdez Ureña, R. Quidant, S. Monneret, J. Polleux, H. Rigneault, Photoinduced heating of nanoparticle arrays, ACS Nano 7 (2013) 6478.

[24] P.C. Lee, D. Meisel, Adsorption and surface-enhanced Raman of dyes on silver and gold sols, J. Phys. Chem. 86 (1982) 3391.

[25] H. Baida, P. Billaud, S. Marhaba, D. Christofilos, E. Cottancin, A. Crut, J. Lermé, P. Maioli, M. Pellarin, M. Broyer, Quantitative determination of the size dependence of surface plasmon resonance damping in single Ag@SiO$_2$ nanoparticles, Nano Lett. 9 (2009) 3463.

[26] X. Li, J.J. Lenhart, Aggregation and dissolution of silver nanoparticles in natural surface water, Environ. Sci. Technol. 46 (2012) 5378.

[27] K.A. Huynh, K.L. Chen, Aggregation kinetics of citrate and polyvinylpyrrolidone coated silver nanoparticles in monovalent and divalent electrolyte solutions, Environ. Sci. Technol. 45 (2011) 5564.

[28] A. Lalisse, G. Tessier, J.r. Plain, G. Baffou, Quantifying the efficiency of plasmonic materials for near-field enhancement and photothermal conversion, J. Phys. Chem. C 119 (2015) 25518.

[29] Y. Sun, Y. Xia, Shape-controlled synthesis of gold and silver nanoparticles, Science 298 (2002) 2176.

[30] V. Amendola, O.M. Bakr, F. Stellacci, A study of the surface plasmon resonance of silver nanoparticles by the discrete dipole approximation method: effect of shape, size, structure, and assembly, Plasmonics 5 (2010) 85.

[31] D.D. Evanoff, G. Chumanov, Synthesis and optical properties of silver nanoparticles and arrays, ChemPhysChem 6 (2005) 1221.

[32] R.A. Tufa, E. Curcio, W. Van Baak, J. Veerman, S. Grasman, E. Fontananova, G. Di Profio, Potential of brackish water and brine for energy generation by salinity gradient power-reverse electrodialysis (SGP-RE), RSC Adv. 4 (2014) 42617.

[33] B.J. Merkel, B. Planer-Friedrich, D. Nordstrom, Groundwater Geochemistry, A Practical Guide to Modeling of Natural and Contaminated Aquatic Systems 2, (2005).